



## ORIGINAL ARTICLE

# Subsidence determination in the Central Valley, California

Marcelo Romero<sup>1</sup> and Mike Mustafa Berber<sup>1\*</sup>

<sup>1</sup>Department of Civil and Geomatics Engineering, California State University, Fresno, 2320 E. San Ramon Avenue, MS/EE 94, Fresno, CA 93740, United States

\*muberber@csufresno.edu

## Abstract

Twenty four hour GNSS (Global Navigation Satellite System) data acquired monthly for 5 years from 8 CORS (Continuously Operating Reference Station) stations in Central Valley, California are processed and vertical velocities of the points are determined. To process GNSS data, online GNSS data processing service APPS (Automatic Precise Positioning Service) is used. GNSS data downloaded from NGS (National Geodetic Survey) CORS are analyzed and subsidence at these points is portrayed with graphics. It is revealed that elevation changes range from 5 mm uplift in the north to 163 mm subsidence in the southern part of the valley.

**Key words:** subsidence, Global Navigation Satellite System, Automatic Precise Positioning Service, elevation changes

## 1 Introduction

Subsidence is a worldwide phenomenon. According to the USGS (United States Geological Survey) in the USA, California, Texas and Florida are the states that suffer from it the most. A major cause of subsidence is exploitation of groundwater. Due to groundwater depletion, water layer holding the ground in place disappears and rocks compact, lowering surface elevation. If this compaction happens in a small spot, subsidence appears in the form of a sinkhole. If it covers large areas like the Central Valley in California, it makes itself visible as a small land drop over time.

According to the USGS, subsidence has been a major concern in the Central Valley of California since the 1950s ([https://ca.water.usgs.gov/land\\_subsidence](https://ca.water.usgs.gov/land_subsidence)). Growing populations and demand on agriculture increased use of groundwater in the valley, thereby exacerbating the already dire situation. USGS studies indicated that by 1970, significant land subsidence (more than 30 cm) had occurred in about half of the valley, or about 13,450 km<sup>2</sup>, and locally, some areas had subsided by as much as 8.5 m. Reduced surface-water availability during 1976–77, 1986–92, 2007–09, and 2012–2015 caused groundwater-pumping increases, declines in water-levels to near or beyond historic lows, and renewed aquifer compaction. In the Central

Valley, subsidence caused costly infrastructure damage such as canal buckling and reduced freeboard on canals and bridges. In some areas, up to 28 cm of land subsidence was measured from 2012 to 2015 (<https://ca.water.usgs.gov/projects/central-valley/land-subsidence-san-joaquin-valley.html>).

Scientists have been putting an effort towards monitoring and understanding subsidence across the globe. For this purpose, various types of instrumentation have been used including InSAR (Interferometric Synthetic Aperture Radar), GPS (Global Positioning System), differential leveling, extensometers, piezometers etc. InSAR relies on satellite images taken at different times. The images are then processed to reveal relative ground-elevation change over time. Nonetheless, InSAR is preferred for projects covering large areas because of the expense and relative ease in processing of the images. An extensometer measures the compaction and expansion of the aquifer system to a specified depth. It is ideal to have extensometer measurements as well; yet, considering drilling and expense for the device itself, they cost a great deal. A piezometer is a specialized well used to measure water levels at specific depths. Again, installation of piezometers is rather expensive. Differential leveling using an automatic or digital level is a precise way of obtaining elevation information providing that the

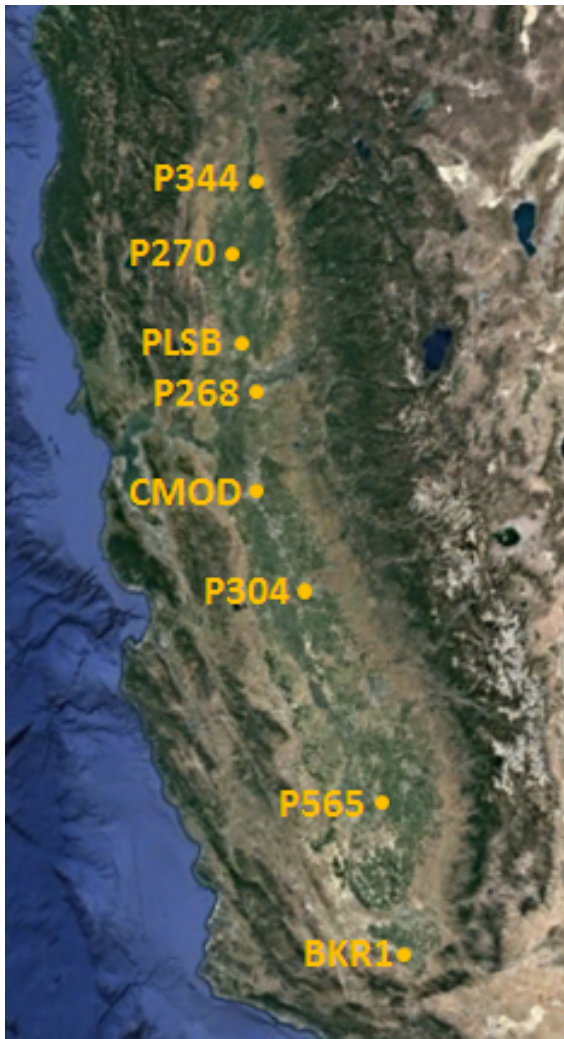


Figure 1. Eight CORS stations in Central Valley, California (image modified from Google)

benchmarks used are out of the subsidence zone. This technique allows carrying an elevation from a known benchmark to other points of interest with high precision. Nevertheless, it is not a feasible technique for large project areas covering a state or a continent since it requires survey crews to take measurements one setup at a time along roads, railroads etc. Whereas, at large scales, GPS is more efficient. GPS provides three dimensional position information of a point, such that by observing variations in the vertical height, subsidence is determined.

Subsidence in the Central Valley, California has been studied by other authors (see for instance Farr et al. (2015)). Summary of recent, historical, and estimated potential for future land subsidence in California is addressed in a report by California Department of Water Resources (2014). In this study, elevations of eight points in the Central Valley of California are determined using 24 hour monthly GNSS data (Figure 1). By examining the elevation changes at these points from 2011 to 2015, subsidence is determined for the Central Valley for this time period.

## 2 Methods

Twenty four hour GNSS (Global Navigation Satellite System) data acquired monthly from 2011 to 2015 are downloaded from

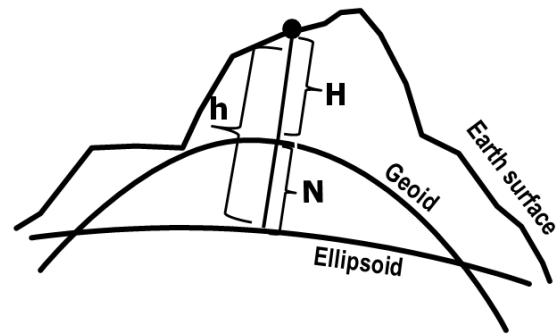


Figure 2. Geoidal height

the NGS (National Geodetic Survey) CORS (Continuously Operating Reference Station) website in RINEX (Receiver Independent Exchange Format) format. Since NGS decimates GNSS data to 30 s sampling rate once the most recent 30 days is over, for this study all the data used have a 30 s sampling rate. Automatic Precise Positioning Service (APPS) is used to process the downloaded data. APPS is currently using GIPSY (GNSS-Inferred Positioning System and Orbit Analysis Simulation Software) version 6.4. A precise point positioning (PPP) technique (Zumberge et al., 1997) is implemented within GIPSY to process GPS phase and pseudorange measurements in RINEX format. By default, the most accurate orbit and clock products are used if available. APPS users may specify the elevation angle cutoff, and by default, the 7.5° elevation angle cutoff is applied. For this study, dual frequency static data are processed using APPS. APPS produces many output files, and coordinate information is provided in a summary file. For more information, the readers are referred to <http://apps.gdgps.net/>.

In the summary file, APPS provides latitude, longitude and ellipsoidal height of a point using WGS84 (World Geodetic System 1984) system. This means that using APPS, ellipsoidal height information is obtained. On the other hand, nature does not follow ellipsoidal height since it is a mathematically defined quantity. Thus, orthometric height is the preferred elevation information to monitor environmental changes such as subsidence even though both ellipsoidal and orthometric height can be used to monitor elevation changes at a point. This is the case specifically for this study because in the end, height differences at the points of interest are determined. On the other hand, if height differences are not used i.e., absolute height value of the points are sought at a certain epoch, one has to be concerned with the geoid model used for those particular orthometric height determinations because different geoid models (<https://www.ngs.noaa.gov/GEOID/>) produce different orthometric heights, which is beyond the scope of this paper. However, interested readers are referred to Wang and Soler (2014) and Lin (2013). NGS has been producing geoid models to convert ellipsoidal height obtained from GPS to orthometric height of a specific vertical datum. In the conterminous United States, North American Vertical Datum of 1988 (NAVD 88) is used. It means that by generating refined geoid models NGS provides geoidal height  $N$  which is the height of the geoid from the reference ellipsoid (see Figure 2):

$$h = H + N, \quad (1)$$

where  $h$  is ellipsoidal height,  $H$  is orthometric height and  $N$  is geoidal height. So, using this formula one can move from ellipsoidal height to orthometric height or vice versa.

### 3 Application and Results

Eight CORS stations in California are used for this study – see Figure 1. While picking these points, care was taken to ensure that these points would not be on mountainous areas and be as close as possible to the north-south cross-section line through the Central Valley. As can be seen in Figure 1, it is not a perfectly straight cross-section line; nonetheless, it is the best obtained using available CORS stations under the above chosen specifications. On the other hand, these points are a seemingly good representation of the Central Valley floor along the north-south direction to depict the subsidence phenomenon in the valley.

By researching available data from the NGS CORS website, it can be found that these points are established at different dates, and data availability varied from point to point. One commonality was that all these points had data since 2011, but again some data was missing here and there. According to USGS, 2011 was not a drought year because most of California's reservoirs were near maximum capacity during the middle of the year. Yet, dry conditions continued from 2011 to 2015 and in the midst of a four-year drought, first-ever statewide water reductions were ordered. Our study timeline coincides with this drought period.

As mentioned above, some data were missing on the NGS CORS website. In addition, some data were not available for the first day of the month. For point P344: for May 2011 the closest data available at the beginning of the month, which is May 7<sup>th</sup>, is accepted, and for February 2013, the earliest data available was February 13<sup>th</sup>. For point PLSB: for July 2011, the earliest data available for the month was for July 7<sup>th</sup>, and for September 2013, September 10<sup>th</sup> data was used. For point CMOD: for March 2013, March 5<sup>th</sup>, for September 2013, September 16<sup>th</sup> and for January 2014, January 8<sup>th</sup> data was used. Although June 2015 data was available on the website, it could not be opened. For BKR1: September 2011 was erroneous and June 2015 data could not be opened.

The first order of business was downloading RINEX data from the NGS CORS website for the eight points used. In order to do so, 24 h RINEX files are downloaded for each point for the beginning of each month; for example, for point P304 one file is downloaded for January 1, February 1, March 1 and so on. Hence, 12 files are downloaded for point P304 for year 2011. Since this study covers a five year period from 2011 to 2015, 60 files are downloaded for this point. Since we used eight points for this work, around 480 RINEX files are processed for this research. To process the RINEX files, APPS software is used.

Since the focus is on the vertical velocities of the points used for this study, only orthometric heights of these points are used. It is well known that GPS height time series contain annual seasonal motion (Blewitt and Lavallée, 2002). The major annual motion is induced from hydrological and atmospheric loading (Akarsu et al., 2015). Various scientific and commercial software are available for annual seasonal motion adjustment. These software use iterative approaches to produce refined estimates of seasonal time series. However, for short periods of data such as the five year GPS data used in this study, a simple adjustment is possible.

The motivation is that for short time series, it is possible to estimate the trend fairly well. There is no unique method to estimate trend in a time series; yet, as long as the trend is consistently increasing or decreasing, for short periods of data analysis, it is typically not very difficult to discern. Therefore, by examining the time series used for this study, it is determined that a second degree polynomial fits well to the data used. In order to do this, using the orthometric heights of the points for each year, a second degree polynomial is determined using MSExcel (see Figure 3). Heights of the points along the trend line are recalculated using the polynomial formula de-

termined for each year. The difference between the original heights and recalculated heights yields the residuals. To calculate seasonal motion adjustments, the average of the residuals for each month are determined for the duration of the data period. For the last step, these adjustment results are subtracted from the original height values. Because it is not possible to show all the results, only the results for point P304 are tabulated in Table 1 as an example.

As can be seen in Figure 3, trend lines are consistently increasing or decreasing for the time period used. By visually inspecting the graphics, it is determined that a second degree polynomial fits well to our data set.

To be able to test the effect of the variance-stabilizing transformation, logged data are also examined. To begin with, logarithms of original height values are computed. Next, using logged data, for each year, a second degree polynomial is determined using Excel. Again, heights of the points along the trend line are recalculated using the polynomial formula determined for each year. The difference between the original heights and recalculated heights yields the residuals. To calculate seasonal motion adjustments, the average of the residuals for each month are determined for the duration of the data period. Finally, these adjustment results are subtracted from original height values. To return to the original scale, the data are used to the power of 10 since base 10 is used for logarithms. The results for point P304 are tabulated in Table 2.

If the results in Table 1 and 2 are compared, it is seen that the results are the same up to third decimal which is an attainable precision using GPS. Since the results are practically the same, logged data is not computed for other points. After removing seasonal motion, changes in elevation at the eight points used in this study are portrayed in Figure 4 for five years.

After removing the seasonal effects, the final elevations of points at the beginning of each year are shown in Table 3.

As can be seen in Table 3, two values for PLSB and one value for P268 are missing. This is the reason that differences in the last row of Table 3 are calculated by subtracting the latest available height value from the earliest available value; for instance, at point P344,  $77.682 - 77.677 = 0.005$  which indicates 5 mm of uplift. As can be seen in Table 3, as we move from north to south (see Figure 1) subsidence increases, which agrees with Figure 5.

As can be seen in Figure 5, major subsidence has been occurring in the southern part of the Central Valley. The image in Figure 5 is produced by the USGS using InSAR, GPS, differential leveling, extensometers, piezometers etc. However, in our study, due to limited resources only GPS data from the NGS CORS website are downloaded and online GPS data processing software is used to analyze the data. On the other hand, our findings are aligned with the USGS results.

### 4 Conclusions

Subsidence along a north-south cross-sectional line in Central Valley, California is examined using 24 h monthly GNSS data collected between 2011 and 2015. From northern Central Valley to the tip of southern Central Valley, 8 points are used for this study. Although other instrumentation such as InSAR, extensometers, piezometers, differential leveling etc. have been used in practice, they are rather expensive to incorporate into a research study. Therefore, in this paper, commonly available GPS data and online GPS data processing software are used to analyze the data sets. For short period time series, it is possible to estimate the trend line by visual inspection as long as the trend is consistently increasing or decreasing. Since, for our study, the time period used is 5 years from 2011 to 2015, vari-

**Table 1.** Orthometric height of point P304 after seasonal motion is removed (m)

Year	Month	Original heights	Recalc. heights	Residuals	Seasonal motion	Seasonal motion removed
2011	1	50.567	50.567	0.000	0.0004	50.5666
2011	2	50.569	50.567	0.002	0.0005	50.5685
2011	3	50.562	50.568	-0.006	-0.0028	50.5645
2011	4	50.572	50.568	0.003	0.0005	50.5714
2011	5	50.565	50.569	-0.004	0.0012	50.5641
2011	6	50.567	50.570	-0.003	-0.0023	50.5695
2011	7	50.579	50.570	0.009	0.0037	50.5752
2011	8	50.571	50.571	0.000	-0.0018	50.5730
2011	9	50.567	50.572	-0.005	-0.0006	50.5678
2011	10	50.568	50.572	-0.005	-0.0050	50.5728
2011	11	50.576	50.573	0.003	-0.0011	50.5773
2011	12	50.573	50.574	-0.001	-0.0002	50.5731
2012	1	50.581	50.578	0.003	0.0004	50.5806
2012	2	50.572	50.574	-0.002	0.0005	50.5719
2012	3	50.567	50.571	-0.004	-0.0028	50.5695
2012	4	50.564	50.568	-0.004	0.0005	50.5632
2012	5	50.568	50.565	0.003	0.0012	50.5665
2012	6	50.567	50.563	0.004	-0.0023	50.5692
2012	7	50.566	50.561	0.005	0.0037	50.5627
2012	8	50.553	50.560	-0.006	-0.0018	50.5550
2012	9	50.547	50.559	-0.011	-0.0006	50.5479
2012	10	50.554	50.558	-0.004	-0.0050	50.5587
2012	11	50.552	50.558	-0.006	-0.0011	50.5531
2012	12	50.554	50.558	-0.004	-0.0002	50.5543
2013	1	50.547	50.549	-0.002	0.0004	50.5461
2013	2	50.548	50.546	0.002	0.0005	50.5475
2013	3	50.541	50.544	-0.003	-0.0028	50.5438
2013	4	50.542	50.541	0.001	0.0005	50.5418
2013	5	50.538	50.538	-0.001	0.0012	50.5365
2013	6	50.536	50.535	0.001	-0.0023	50.5386
2013	7	50.533	50.532	0.001	0.0037	50.5293
2013	8	50.526	50.529	-0.003	-0.0018	50.5278
2013	9	50.528	50.526	0.003	-0.0006	50.5288
2013	10	50.512	50.522	-0.010	-0.0050	50.5170
2013	11	50.519	50.518	0.001	-0.0011	50.5203
2013	12	50.516	50.515	0.002	-0.0002	50.5166
2014	1	50.518	50.515	0.003	0.0004	50.5174
2014	2	50.507	50.513	-0.005	0.0005	50.5067
2014	3	50.513	50.510	0.003	-0.0028	50.5159
2014	4	50.506	50.507	-0.001	0.0005	50.5051
2014	5	50.511	50.504	0.006	0.0012	50.5093
2014	6	50.493	50.501	-0.008	-0.0023	50.4949
2014	7	50.497	50.498	-0.001	0.0037	50.4937
2014	8	50.497	50.495	0.002	-0.0018	50.4990
2014	9	50.497	50.492	0.005	-0.0006	50.4978
2014	10	50.486	50.489	-0.003	-0.0050	50.4908
2014	11	50.484	50.486	-0.002	-0.0011	50.4846
2014	12	50.484	50.483	0.001	-0.0002	50.4838
2015	1	50.481	50.483	-0.002	0.0004	50.4809
2015	2	50.485	50.479	0.006	0.0005	50.4847
2015	3	50.472	50.476	-0.004	-0.0028	50.4743
2015	4	50.476	50.472	0.003	0.0005	50.4750
2015	5	50.470	50.469	0.001	0.0012	50.4689
2015	6	50.460	50.466	-0.006	-0.0023	50.4623
2015	7	50.467	50.463	0.004	0.0037	50.4632
2015	8	50.458	50.460	-0.002	-0.0018	50.4595
2015	9	50.462	50.457	0.005	-0.0006	50.4623
2015	10	50.451	50.454	-0.003	-0.0050	50.4563
2015	11	50.450	50.451	-0.001	-0.0011	50.4514
2015	12	50.450	50.449	0.001	-0.0002	50.4499

**Table 2.** Orthometric height of point P304 using logged data (m)

Year	Month	Original heights	Logged heights	Recalc. heights	Residuals	Seasonal motion	Logged results	Final heights
2011	1	50.567	1.7039	1.7039	0.0000	0.0000	1.7039	50.5664
2011	2	50.569	1.7039	1.7039	0.0000	0.0000	1.7039	50.5684
2011	3	50.562	1.7038	1.7039	-0.0001	0.0000	1.7038	50.5643
2011	4	50.572	1.7039	1.7039	0.0000	0.0000	1.7039	50.5712
2011	5	50.565	1.7039	1.7039	-0.0001	0.0000	1.7038	50.5638
2011	6	50.567	1.7039	1.7039	-0.0001	0.0000	1.7039	50.5691
2011	7	50.579	1.7040	1.7039	0.0000	0.0000	1.7039	50.5747
2011	8	50.571	1.7039	1.7039	0.0000	0.0000	1.7039	50.5723
2011	9	50.567	1.7039	1.7039	-0.0001	0.0000	1.7039	50.5669
2011	10	50.568	1.7039	1.7040	-0.0001	0.0000	1.7039	50.5715
2011	11	50.576	1.7039	1.7040	0.0000	0.0000	1.7039	50.5757
2011	12	50.573	1.7039	1.7040	0.0000	0.0000	1.7039	50.5713
2012	1	50.581	1.7040	1.7040	0.0000	0.0000	1.7040	50.5804
2012	2	50.572	1.7039	1.7039	0.0000	0.0000	1.7039	50.5718
2012	3	50.567	1.7039	1.7039	0.0000	0.0000	1.7039	50.5693
2012	4	50.564	1.7038	1.7039	0.0000	0.0000	1.7038	50.5630
2012	5	50.568	1.7039	1.7038	0.0000	0.0000	1.7039	50.5662
2012	6	50.567	1.7039	1.7038	0.0001	0.0000	1.7039	50.5688
2012	7	50.566	1.7039	1.7038	0.0001	0.0000	1.7038	50.5622
2012	8	50.553	1.7037	1.7037	0.0000	0.0000	1.7038	50.5543
2012	9	50.547	1.7037	1.7037	0.0000	0.0000	1.7037	50.5470
2012	10	50.554	1.7038	1.7037	0.0001	0.0000	1.7038	50.5574
2012	11	50.552	1.7037	1.7037	0.0001	0.0000	1.7037	50.5515
2012	12	50.554	1.7038	1.7037	0.0001	0.0000	1.7037	50.5525
2013	1	50.547	1.7037	1.7037	0.0000	0.0000	1.7037	50.5459
2013	2	50.548	1.7037	1.7037	0.0000	0.0000	1.7037	50.5474
2013	3	50.541	1.7036	1.7036	0.0000	0.0000	1.7037	50.5436
2013	4	50.542	1.7037	1.7036	0.0000	0.0000	1.7036	50.5416
2013	5	50.538	1.7036	1.7036	0.0000	0.0000	1.7036	50.5362
2013	6	50.536	1.7036	1.7036	0.0000	0.0000	1.7036	50.5382
2013	7	50.533	1.7036	1.7035	0.0000	0.0000	1.7035	50.5288
2013	8	50.526	1.7035	1.7035	0.0000	0.0000	1.7035	50.5271
2013	9	50.528	1.7035	1.7035	0.0001	0.0000	1.7035	50.5279
2013	10	50.512	1.7034	1.7034	0.0000	0.0000	1.7034	50.5157
2013	11	50.519	1.7035	1.7034	0.0000	0.0000	1.7035	50.5187
2013	12	50.516	1.7034	1.7034	0.0001	0.0000	1.7034	50.5148
2014	1	50.518	1.7034	1.7034	0.0001	0.0000	1.7034	50.5172
2014	2	50.507	1.7034	1.7034	0.0000	0.0000	1.7033	50.5066
2014	3	50.513	1.7034	1.7033	0.0001	0.0000	1.7034	50.5157
2014	4	50.506	1.7033	1.7033	0.0000	0.0000	1.7033	50.5049
2014	5	50.511	1.7034	1.7033	0.0001	0.0000	1.7034	50.5090
2014	6	50.493	1.7032	1.7033	0.0000	0.0000	1.7032	50.4945
2014	7	50.497	1.7033	1.7033	0.0000	0.0000	1.7032	50.4932
2014	8	50.497	1.7033	1.7032	0.0000	0.0000	1.7033	50.4983
2014	9	50.497	1.7033	1.7032	0.0001	0.0000	1.7033	50.4969
2014	10	50.486	1.7032	1.7032	0.0000	0.0000	1.7032	50.4895
2014	11	50.484	1.7031	1.7032	0.0000	0.0000	1.7031	50.4830
2014	12	50.484	1.7032	1.7031	0.0000	0.0000	1.7031	50.4820
2015	1	50.481	1.7031	1.7032	0.0000	0.0000	1.7031	50.4807
2015	2	50.485	1.7032	1.7031	0.0000	0.0000	1.7032	50.4846
2015	3	50.472	1.7030	1.7031	-0.0001	0.0000	1.7031	50.4741
2015	4	50.476	1.7031	1.7031	0.0000	0.0000	1.7031	50.4748
2015	5	50.470	1.7030	1.7031	0.0000	0.0000	1.7030	50.4686
2015	6	50.460	1.7029	1.7030	-0.0001	0.0000	1.7030	50.4619
2015	7	50.467	1.7030	1.7030	0.0000	0.0000	1.7030	50.4627
2015	8	50.458	1.7029	1.7030	-0.0001	0.0000	1.7029	50.4588
2015	9	50.462	1.7030	1.7030	0.0000	0.0000	1.7030	50.4614
2015	10	50.451	1.7029	1.7030	-0.0001	0.0000	1.7029	50.4550
2015	11	50.450	1.7029	1.7029	-0.0001	0.0000	1.7029	50.4498
2015	12	50.450	1.7029	1.7029	-0.0001	0.0000	1.7028	50.4481

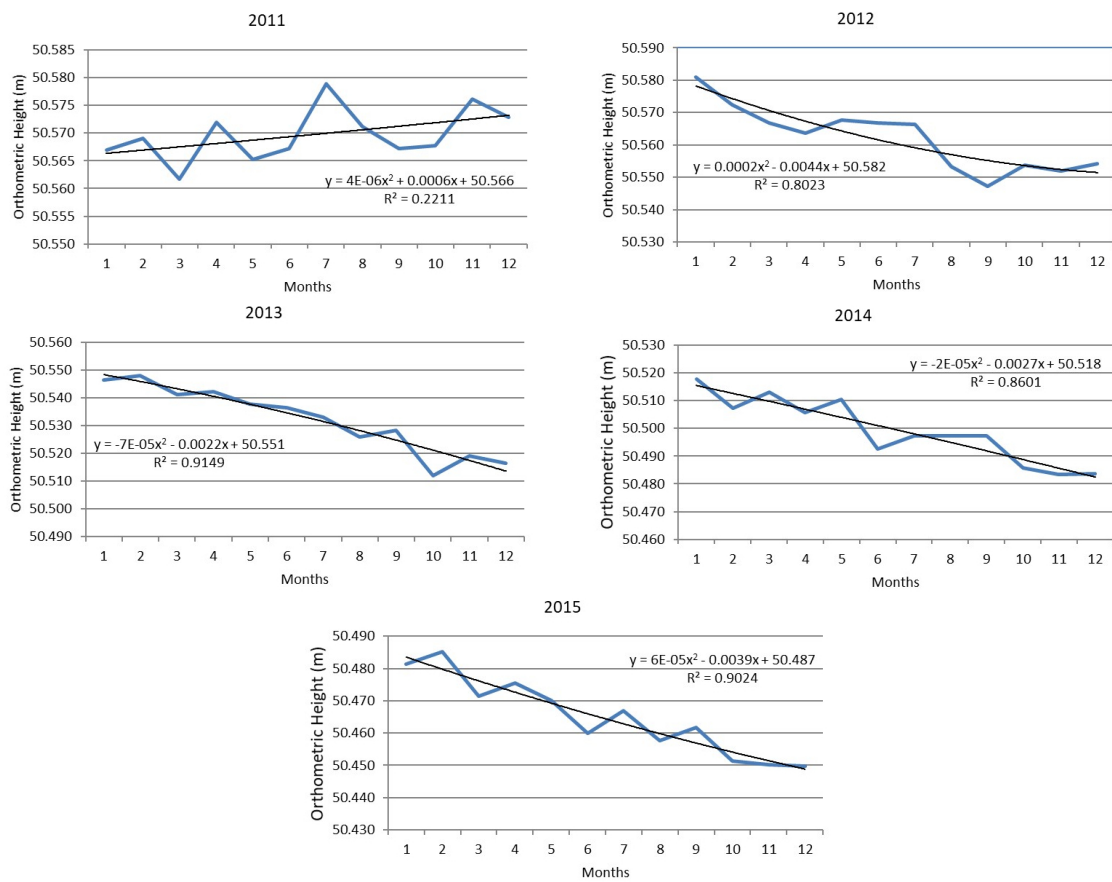
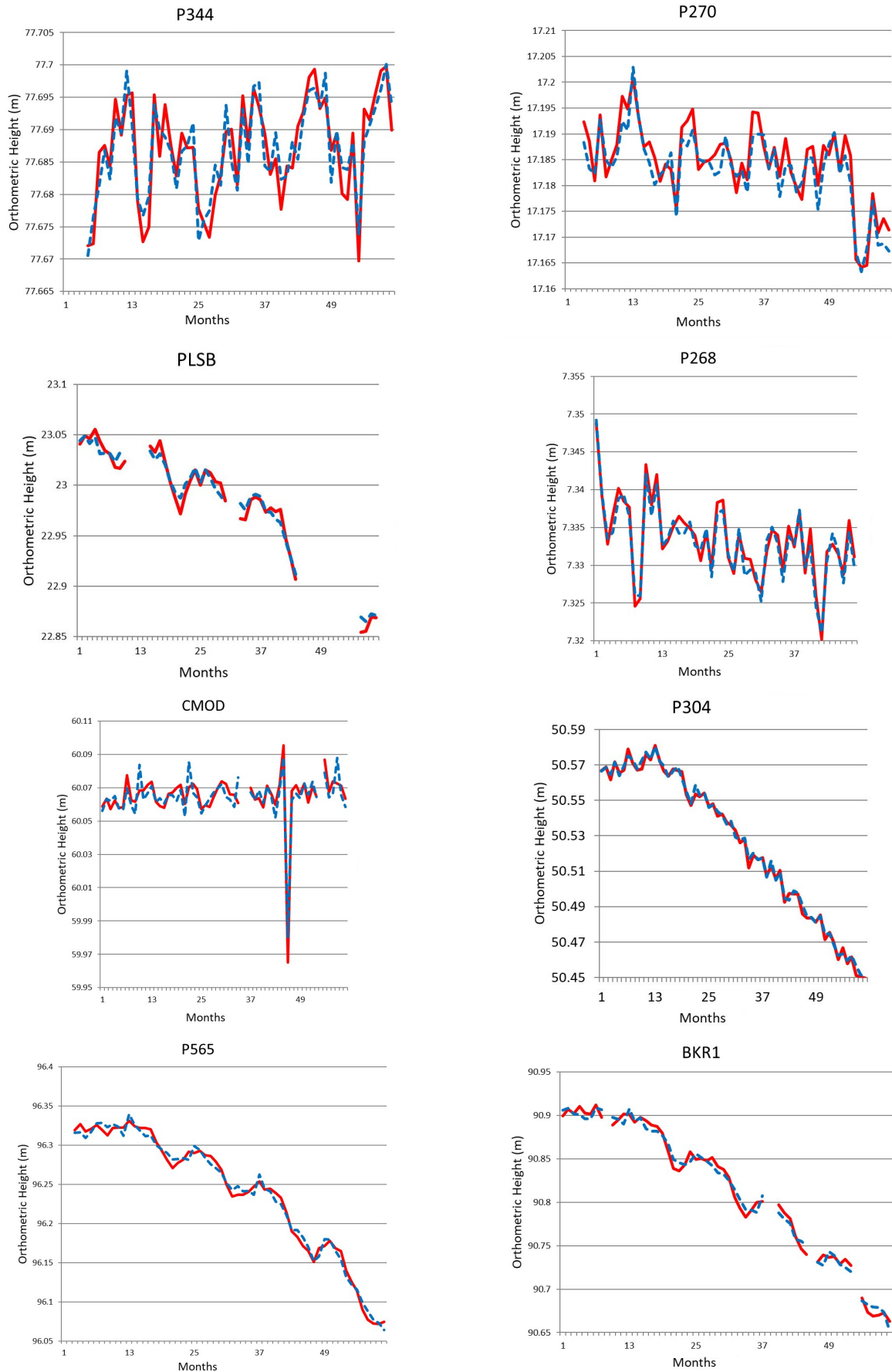


Figure 3. Calculated trend lines for point P304 with second order polynomials

Table 3. Final elevations at the beginning of each year for the eight points used in this study (m)

Year	P344	P270	PLSB	P268	CMOD	P304	P565	BKR1
2011	77.677	17.191	23.044		60.056	50.567	96.328	90.906
2012	77.691	17.203		7.349	60.071	50.581	96.340	90.908
2013	77.673	17.185	23.003	7.333	60.055	50.546	96.299	90.856
2014	77.684	17.190	22.989	7.332	60.067	50.517	96.263	90.808
2015	77.682	17.188		7.333	60.064	50.481	96.180	90.743
Difference	0.005	-0.003	-0.055	-0.016	0.008	-0.086	-0.148	-0.163



**Figure 4.** Subsidence at the eight points used in this study after removing seasonal motion. In the graphs, the solid red line represents the original height values and the dashed blue line represents the elevations after seasonal motion is removed. The horizontal axis is scaled in months for five years from 1 to 60, and the vertical axis shows the height in meters.

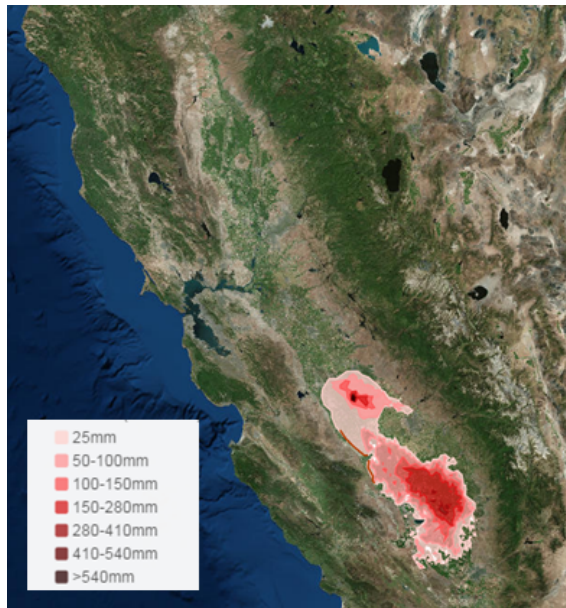


Figure 5. Subsidence contours in the Central Valley of California (image from USGS: [https://ca.water.usgs.gov/land\\_subsidence/california-subsidence-areas.html](https://ca.water.usgs.gov/land_subsidence/california-subsidence-areas.html))

ous polynomials beginning with first degree and then second degree and then third, fourth etc. are examined. It is determined that a second degree polynomial fits well to our data set. To test the effect of the variance-stabilizing transformation, logged data are also examined. Nevertheless, it is seen that the results are the same up to third decimal between using a second degree polynomial and logged data. Thus, logged data is not used. At the end of the analyses, it is found that from north to south, elevation changes range from 5 mm uplift to 163 mm subsidence. This means that subsidence is more pervasive in the southern part of the valley, and this is in agreement with the USGS determinations. Our findings are aligned with the USGS results in spite of the fact that only GPS data are used.

## Acknowledgements

The authors would like to thank the NGS CORS for GNSS data available for online downloading free of charge from their website. The authors also thank JPL APPS for providing the online GNSS data processing service. The authors would like to thank Stephen Castillo for editing the manuscript.

## References

- Akarsu, V., Sanli, D., and Arslan, E. (2015). Accuracy of velocities from repeated GPS measurements. *Natural Hazards and Earth System Sciences*, 15(4):875–884, doi:10.5194/nhess-15-875-2015.
- Blewitt, G. and Lavallée, D. (2002). Effect of annual signals on geodetic velocity. *Journal of Geophysical Research: Solid Earth*, 107(B7):ETG 9–1–ETG 9–11, doi:10.1029/2001JB000570.
- California Department of Water Resources (2014). Summary of recent, historical, and estimated potential for future land subsidence in California. [https://water.ca.gov/LegacyFiles/groundwater/docs/Summary\\_of\\_Recent\\_Historical\\_Potential\\_Subsidence\\_in\\_CA\\_Final\\_with\\_Appendix.pdf](https://water.ca.gov/LegacyFiles/groundwater/docs/Summary_of_Recent_Historical_Potential_Subsidence_in_CA_Final_with_Appendix.pdf). Accessed: 20.12.2018.
- Farr, T. G., Jones, C., and Liu, Z. (2015). *Progress report: subsidence in the Central Valley, California*. Jet Propulsion Laboratory, California Institute of Technology. Accessed: 20.12.2018.
- Lin, L.-S. (2013). Orthometric height improvement in Tainan City using RTK GPS and local geoid corrector surface models. *Journal of surveying engineering*, 140(1):35–43, doi:10.1061/(ASCE)SU.1943-5428.0000114.
- Wang, G. and Soler, T. (2014). Measuring land subsidence using GPS: ellipsoid height versus orthometric height. *Journal of Surveying Engineering*, 141(2):05014004, doi:10.1061/(ASCE)SU.1943-5428.0000137.
- Zumberge, J., Heflin, M., Jefferson, D., Watkins, M., and Webb, F. H. (1997). Precise point positioning for the efficient and robust analysis of GPS data from large networks. *Journal of geophysical research: solid earth*, 102(B3):5005–5017, doi:10.1029/96JB03860.